Quartz: Superoptimization of Quantum Circuits

Mingkuan Xu
Carnegie Mellon University
Pittsburgh, PA, USA
mingkuan@cmu.edu

Zikun Li
University of California, Los Angeles
Los Angeles, CA, USA
lizikun_@outlook.com

Oded Padon
VMware Research
Palo Alto, CA, USA
oded.padon@gmail.com

Sina Lin
Microsoft
Mountain View, CA, USA
silin@microsoft.com

Jessica Pointing
University of Oxford
Oxford, United Kingdom
jessica.pointing@physics.ox.ac.uk

Auguste Hirth
University of California, Los Angeles
Los Angeles, CA, USA
ahirth@g.ucla.edu

Henry Ma
University of California, Los Angeles
Los Angeles, CA, USA
hetm@g.ucla.edu

Jens Palsberg
University of California, Los Angeles
Los Angeles, CA, USA
palsberg@cs.ucla.edu

Alex Aiken
Stanford University
Stanford, CA, USA
aiken@cs.stanford.edu

Umut A. Acar
Carnegie Mellon University
Pittsburgh, PA, USA
umut@cs.cmu.edu

Zhihao Jia
Carnegie Mellon University
Pittsburgh, PA, USA
zhihao@cmu.edu

Abstract

Existing quantum compilers optimize quantum circuits by applying circuit transformations designed by experts. This approach requires significant manual effort to design and implement circuit transformations for different quantum devices, which use different gate sets, and can miss optimizations that are hard to find manually. We propose Quartz, a quantum circuit superoptimizer that *automatically* generates and verifies circuit transformations for arbitrary quantum gate sets. For a given gate set, Quartz generates candidate circuit transformations by systematically exploring small circuits and verifies the discovered transformations using an automated theorem prover. To optimize a quantum circuit, Quartz uses a cost-based backtracking search that applies the verified transformations to the circuit. Our evaluation on three popular gate sets shows that Quartz can effectively generate and verify transformations for different gate sets. The generated transformations cover manually designed transformations used by existing optimizers and also include new transformations. Quartz is therefore able to optimize a broad range of circuits for diverse gate sets, outperforming or matching the performance of hand-tuned circuit optimizers.

1 Introduction

Quantum computing comes in many shapes and forms. There are over a dozen proposals for realizing quantum computing in practice, and nearly all these proposals support different kinds of quantum operations, i.e., instruction set architectures (ISAs). The increasing diversity in quantum processors makes it challenging to design optimizing compilers for quantum programs, since the compilers must consider a variety of ISAs and carry optimizations specific to different ISAs.

To reduce the execution cost of a quantum circuit, the most common form of optimization is *circuit transformations* that substitute a subcircuit matching a specific pattern with a functionally equivalent new subcircuit with improved performance (e.g., using fewer quantum gates). Existing quantum compilers generally rely on circuit transformations manually designed by experts and applied greedily. For example, Qiskit [5] and t|ket⟩ [28] use greedy rule-based strategies to optimize a quantum circuit and perform circuit transformations whenever applicable. voqc [15] formally verifies

circuit transformations but still requires users manually specify them. Although rule-based transformations can reduce the cost of a quantum circuit, they have two key limitations.

First, because existing optimizers rely on domain experts to design transformations, they require significant human effort and may also miss subtle optimizations that are hard to discover manually, resulting in sub-optimal performance.

Second, circuit transformations designed for one quantum device do not directly apply to other devices with different ISAs, which is problematic in the emerging diverse quantum computing landscape. For example, IBMQX5 [12] supports the U_1, U_2, U_3 and $CNOT$ gates, while Rigetti Agave [26] supports the $R_x(\pm\frac{\pi}{2})$, $R_x(\pi)$, $R_z(\lambda)$, and CZ gates. As a result, circuit transformations tailored for IBMQX5 cannot optimize circuits on Rigetti Agave, and vice versa.

Recently, Quanto [25] proposed to automatically discover transformations by computing concrete matrix representations of circuits. Its main restriction is that it does not discover symbolic transformations, which are needed to deal with common *parametric* quantum gates in a general way.

This paper presents Quartz, a quantum circuit superoptimizer that automatically generates and verifies symbolic circuit transformations for arbitrary gate sets, including parametric gates. Quartz provides two key advantages over existing quantum circuit optimizers. First, for a given set of gates, Quartz generates symbolic circuit transformations and formally verifies their correctness in a fully *automated* way, without any manual effort to design or implement transformations. Second, Quartz explores a more comprehensive set of circuit transformations by discovering *all* possible transformations up to a certain size, outperforming existing optimizers with manually designed transformations.

ECC sets. We introduce *equivalent circuit classes* (ECCs) as a compact way to represent circuit transformations. Each ECC is a set of functionally equivalent circuits, and two circuits from an ECC form a valid transformation. We say that a transformation is *subsumed* by an *ECC set* (a set of ECCs) if the transformation can be decomposed into a sequence of transformations, each of which is a pair of circuits from the same ECC in the ECC set. We use (n, q)-*completeness* to assess the comprehensiveness of an ECC set—an ECC set is (n, q)-complete if it subsumes *all* valid transformations between circuits with at most n gates and q qubits.

Overview. Figure 1 shows an overview of Quartz, which uses an *interleaving* approach: it iteratively generates candidate circuits, eliminates redundancy, and verifies equivalences. In the j-th iteration, Quartz generates a (j, q)-complete ECC set based on the $(j-1, q)$-complete ECC set from the previous iteration. The generated ECC set may contain redundant transformations. We introduce RepGen, a representative-based circuit generation algorithm that uses a $(j-1, q)$-complete ECC set to generate circuits for a (j, q)-complete ECC set with fewer redundancies. The circuits are
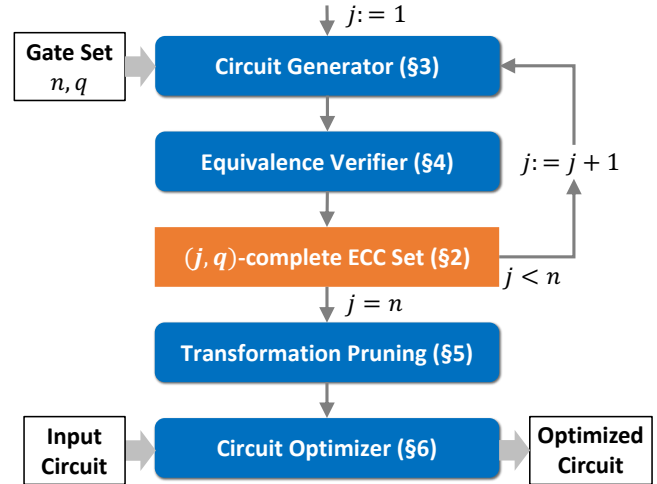

Figure 1. Quartz overview.

sent to the *circuit equivalence verifier*, which formally verifies equivalence between circuits and produces a (j, q)-complete ECC set. After generating an (n, q)-complete ECC set, Quartz employs several pruning techniques to further eliminate redundancies. Finally, Quartz's *circuit optimizer* applies the discovered transformations to optimize an input circuit.

Circuit Generator. Given a gate set and a circuit size n, Quartz's *circuit generator* generates candidate circuits of size at most n using the RepGen algorithm, which avoids generating all possible circuits (of which there are exponentially many) while ensuring (n, q)-completeness. To this end, RepGen iteratively constructs ECC sets, from smaller to larger. For each ECC, RepGen selects a *representative circuit* and constructs larger circuits by extending these representatives.

To discover equivalences between circuits, RepGen uses random inputs to assign a *fingerprint* (i.e., a hash) to each circuit and checks only the circuits with the same fingerprint. We prove an upper bound on the running time of RepGen in terms of the number of representatives generated. For the gate sets considered in our evaluation, RepGen reduces the number of circuits in an ECC set by one to three orders of magnitudes while maintaining (n, q)-completeness.

Circuit Equivalence Verifier. Quartz's *circuit equivalence verifier* checks if two potentially equivalent circuits are indeed functionally equivalent. A major challenge is dealing with gates that take one or multiple parameters (e.g., U_1, U_2, and U_3 in IBMQX5, and R_z in Rigetti Agave). For candidate equivalent circuits, Quartz checks whether they are functionally equivalent for arbitrary combinations of parameter assignments and quantum states. To this end, Quartz computes symbolic matrix representations of the circuits. The resulting verification problem involves trigonometric functions and, in the general case, a quantifier alternation;

Quartz soundly eliminates both and reduces circuit equivalence checking to SMT solving for quantifier-free formulas over the theory of nonlinear real arithmetic. The resulting SMT queries are efficiently solved by the Z3 [10] SMT solver.

Circuit Pruning. Having generated an (n, q)-complete ECC set, Quartz optimizes circuits by applying the transformations specified by the ECC set. To improve the efficiency of this optimization step, described next, Quartz applies several pruning techniques to eliminate redundant transformations.

Circuit Optimizer. Quartz's *circuit optimizer* uses a cost-based backtracking search algorithm adapted from TASO [17] to apply the verified transformations. The search is guided by a cost model that compares the performance of different candidate circuits (in our experiments the cost is given by number of gates). Quartz targets the *logical optimization* stage in quantum circuit compilation. That is, Quartz operates before *qubit mapping* where logical qubits are mapped to physical qubits while respecting hardware constraints [11, 31].

Evaluation. Our evaluation on three gate sets derived from existing quantum processors shows that Quartz can generate and verify circuit transformations for different gate sets in under 30 minutes (using 128 cores). For logical circuit optimization, Quartz matches and often outperforms existing optimizers. On a benchmark of 26 circuits, Quartz obtains average gate count reductions of 29%, 30%, and 49% for the Nam, IBM, and Rigetti gate sets; the corresponding reductions by existing optimizers are 27%, 23%, and 39%.

2 Symbolic Quantum Circuits

To support parametric gates, Quartz introduces *symbolic quantum circuits* and *circuit transformations*. The latter are represented compactly using *equivalent circuit classes* (ECCs). This section introduces these concepts.

Quantum circuits. Quantum programs are represented as *quantum circuits* [24], as shown in Figure 2a, where each horizontal wire represents a *qubit*, and boxes on these wires represent *quantum gates*. The semantics of a quantum circuit over q qubits is given by a $2^q \times 2^q$ unitary complex matrix. This matrix can be computed from matrices of individual gates in a compositional manner, using matrix multiplications (for sequential composition of subcircuits that operate on the same qubits) and tensor products (for parallel composition of subcircuits that operate on different qubits). For example, the matrix for the circuit of Figure 2a is $(CNOT \otimes I) \cdot (U_2(\frac{\pi}{2}, \pi) \otimes CNOT) \cdot (U_1(-\pi) \otimes H \otimes H)$.

A circuit C' is a *subcircuit* of C if, for some qubit permutation, the matrix computation for C can be structured as $\_ \cdot (M_{C'} \otimes I \otimes \cdots \otimes I) \cdot \_$, where $M_{C'}$ is the matrix for C'. For example, the green box in Figure 2a highlights a subcircuit, while the red dashed area is not a subcircuit. The subcircuit notion is invariant under qubit permutation; e.g., the X and

(a) Quantum circuit. **(b)** Symbolic Quantum circuit.

(c) Transformation fusing two R_z gates across CZ and X gates.
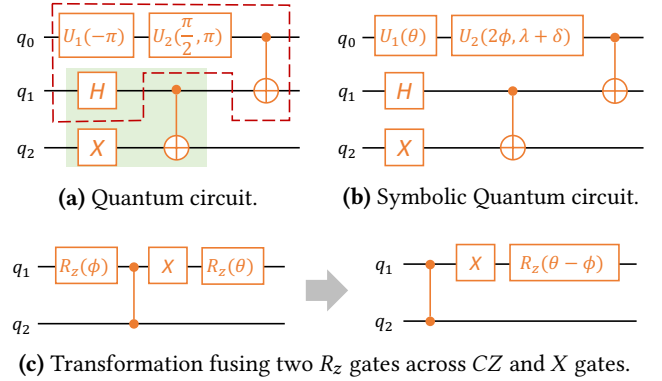
Figure 2. Quantum circuits and transformations. The green highlighted box in (a) is a subcircuit, while the red dashed area is not; the $U_1(-\pi)$ and X gates also form a subcircuit.

U_1 gates in Figure 2a also form a subcircuit. A circuit's matrix is invariant under replacing one subcircuit with another that has the same matrix (but possibly different gates), which underpins peephole optimization for quantum circuits.
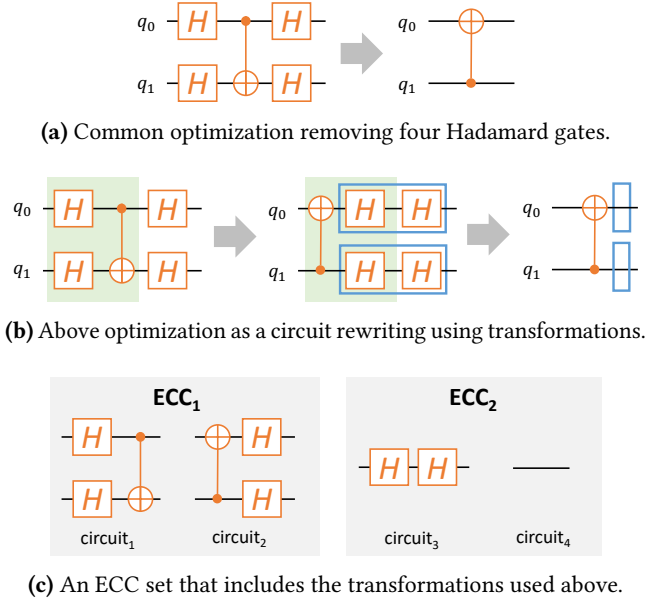
Many gates supported by modern quantum devices take real-valued parameters. For example, the IBM quantum device supports the U_1 gate which takes one parameter and rotates a qubit about the x-axis (on the Bloch sphere), and the U_2 gate which takes two parameters for rotating about the x- and z-axes. The matrix representations of U_1 and U_2 are:

$$U_1(\theta) = \begin{pmatrix} 1 & 0 \\ 0 & e^{i\theta} \end{pmatrix} \quad U_2(\phi, \lambda) = \frac{1}{\sqrt{2}} \begin{pmatrix} 1 & -e^{i\lambda} \\ e^{i\phi} & e^{i(\phi+\lambda)} \end{pmatrix} \quad (1)$$

Symbolic circuits. To support superoptimization of circuits with parametric gates, Quartz discovers transformations between *symbolic quantum circuits*, as shown in Figure 2b, which include (symbolic) parameters (θ, ϕ, λ, δ, etc.) and arithmetic operations on these parameters, and are formalized below. Using such circuits, Quartz can represent transformations such as the one illustrated in Figure 2c.

The semantics of a *symbolic quantum circuit*, denoted $[\![\cdot]\!]$, has type $[\![C]\!]: \mathbb{R}^m \to \mathbb{C}^{2^q \times 2^q}$ where C is a circuit over m (symbolic) parameters and q qubits. For a vector of parameter values $\vec{p} \in \mathbb{R}^m$, $[\![C]\!](\vec{p})$ is a $2^q \times 2^q$ unitary complex matrix representing a (concrete) quantum circuit over q qubits. For example, eq. (1) can be seen as defining the semantics of U_1 and U_2 as single-gate symbolic quantum circuits. The semantics of a multi-gate symbolic circuit (e.g., Figure 2b) is derived from that of single-gate circuits using matrix multiplications and tensor products exactly as for concrete circuits. Henceforth, we use *circuits* to mean symbolic quantum circuits.

Circuit equivalence and transformations. In quantum computing, the states $|\psi\rangle$ and $e^{i\beta} |\psi\rangle$ ($\beta \in \mathbb{R}$) are *equivalent up to a global phase*, and from an observational point of view they are identical [24]. This leads to the following circuit-equivalence definition that underlies Quartz's optimization.

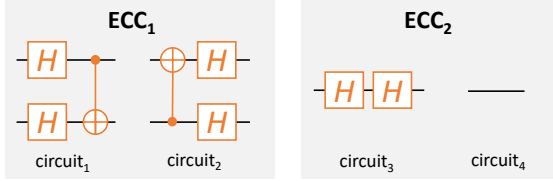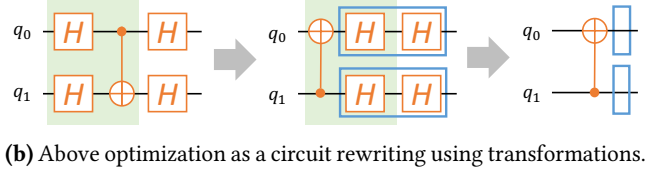**(a)** Common optimization removing four Hadamard gates.

(b) Above optimization as a circuit rewriting using transformations.

(c) An ECC set that includes the transformations used above.

Figure 3. Illustrating optimization via transformations.

Definition 1 (Circuit Equivalence). *Two symbolic quantum circuits C_1 and C_2 are* equivalent *if:*

$$\forall \vec{p} \in \mathbb{R}^m. \; \exists \beta \in \mathbb{R}. \; [\![C_1]\!](\vec{p}) = e^{i\beta}[\![C_2]\!](\vec{p}). \qquad (2)$$

That is, two circuits are equivalent if for every valuation of the parameters they differ only by a phase factor. The phase factor may in some cases be constant, but generally it may be different for different parameter values. For example, the equivalence between U_1 and R_z gates ($U_1(\theta) = e^{i\theta/2}R_z(\theta)$) requires a parameter-dependent phase factor. Crucially for peephole optimization, circuit equivalence is invariant under replacing a subcircuit with an equivalent subcircuit.

A *circuit transformation* (C_T, C_R) is a pair of distinct equivalent circuits, where C_T is a *target circuit* to be matched with a subcircuit of the circuit being optimized, and C_R is a *rewrite circuit* that can replace the target circuit while maintaining equivalence of the optimized circuit and the input circuit. Figure 2c illustrates a circuit transformation.

Equivalent Circuit Classes. Quartz uses *equivalent circuit classes* (ECCs), to represent many circuit transformations compactly. An ECC is a set of equivalent circuits. A transformation is *included* in an ECC if both its target and rewrite circuits are in the ECC. ECCs provide a compact representation of circuit transformations: an ECC with x circuits includes $x(x-1)$ transformations.

A *circuit rewriting* is a sequence of applications of circuit transformations, which Quartz uses for optimization as illustrated in Figure 3. Figure 3a shows a common optimization that removes four Hadamard gates (i.e., H) by flipping a *CNOT* gate. Figure 3b shows how to perform this optimization as a circuit rewriting consisting of three (more

basic) circuit transformations, which are instances of the two transformations specified by the ECC set in Figure 3c.

Completeness for ECC sets. For any number of gates n, qubits q, and parameters m, we assume a *finite* set $C^{(n,q,m)}$ of circuits that can be constructed with at most n gates over q qubits and m parameters. The collection $\{C^{(n,q,m)}\}_{n,q,m\in\mathbb{N}}$ is determined by the *gate set* $\mathcal{G}$ (finite set of possibly parametric gates) as well as a specification Σ of how parameter expressions may be constructed; e.g., a finite set of arithmetic operations and some bounds on the depth of expressions or the number of times each parameter can be used, ensuring finiteness of every $C^{(n,q,m)}$. Henceforth, we fix the gate set $\mathcal{G}$, the parameter-expression specification Σ, and the number of parameters m; and elide m by writing $C^{(n,q)}$.

A transformation (C_T, C_R) is *subsumed* by an ECC set if there is a circuit rewriting from C_T to C_R that only uses transformations included in the ECC set.

Definition 2 ((n, q)-Completeness). *Given $\mathcal{G}$, Σ, and m as above, an ECC set is (n, q)-complete (for $\mathcal{G}$, Σ, and m) if it subsumes all circuit transformations over $C^{(n,q)}$.*

An (n, q)-complete ECC set can be used to rewrite any two equivalent circuits with at most n gates over q qubits to each other. Any ECC set is by default $(0, q)$-complete because any transformation involves at least one gate in the target or rewrite circuits. An ECC set is $(1, q)$-complete if it subsumes all possible transformations between single gates. Sections 3 to 5 describe our approach for constructing a verified (n, q)-complete ECC set.

3 Circuit Generator

Quartz builds an (n, q)-complete ECC set using the RepGen algorithm, developed in this section, which interleaves circuit generation and equivalence verification (see Figure 1).

3.1 The RepGen Algorithm

A straightforward way to generate an (n, q)-complete ECC set is to examine all circuits in $C^{(n,q)}$, but there are exponentially many such circuits. To tackle this challenge, RepGen uses *representative-based circuit generation*, which significantly reduces the number of circuits considered. The key idea is to extend a (j, q)-complete ECC set to a $(j + 1, q)$-complete one by selecting a representative circuit for each ECC and using these representatives to build larger circuits.

Sequence representation for circuits. RepGen represents a circuit as a sequence of instructions that reflects a topological ordering of its gates (i.e., respecting dependencies). E.g., a possible sequence for the circuit in Figure 2b is: U1 θ 0; U2 2ϕ $\lambda+\delta$ 0; H 1; X 2; CNOT 1 2; CNOT 0 1. We write () for the empty sequence and $L.(g\,\iota)$ for appending gate $g \in \mathcal{G}$ with arguments ι (parameter expressions and qubit indices) to sequence L; e.g., for the second instruction above $g = $ U2 and $\iota = (2\phi, \lambda+\delta, 0)$. Different sequences may

Algorithm 1 RepGen.

1: **Input:** Number of gates n and qubits q.
2: **Output:** (n, q)-complete ECC set.
3: $\mathcal{D} = \emptyset$ // Hash table of circuit sets indexed by fingerprint
4: $\mathcal{D}[\text{FingerPrint}(())] = \{()\}$ // Initialize with empty circuit
5: $\mathcal{R}_0 = \{()\}$ // Representatives with 0 gates
6: $\mathcal{S}_0 = \emptyset$ // $(0, q)$-complete ECC set
7: **for** $j = 1$ **to** n **do**
8:     // Step 1: construct circuits (sequences) with j gates
9:     **for** each circuit $L \in \mathcal{R}_{j-1}$ such that $|L| = j - 1$ **do**
10:         **for** each gate $g \in \mathcal{G}$ **do**
11:             **for** each ι such that $L' = L.(g\ \iota)$ satisfies Σ **do**
12:                 **if** $\text{DropFirst}(L') \in \mathcal{R}_{j-1}$ **then**
13:                     add L' to $\mathcal{D}[\text{FingerPrint}(L')]$
14:     // Step 2: examine circuits with equal fingerprints
15:     $\mathcal{S}_j = \bigcup\{\text{Eccify}(\gamma) : \gamma = \mathcal{D}[f] \text{ for some } f\}$
16:     $\mathcal{R}_j = \{min(\mathcal{E}) : \mathcal{E} \in \mathcal{S}_j\}$ // Under $\prec$ (Definition 3)
17: **return** $\{\mathcal{E} \in \mathcal{S}_n : |\mathcal{E}| \geq 2\}$ // Ignore singleton ECCs
18:
19: // Partition circuits into verified ECCs
20: **function** Eccify(γ)
21:     $\widehat{\mathcal{S}} = \emptyset$ // Set of ECCs for circuits in γ
22:     **for** each circuit $C \in \gamma$ **do**
23:         **if** C is equivalent to a circuit in ECC $\mathcal{E} \in \widehat{\mathcal{S}}$ **then**
24:             $\widehat{\mathcal{S}} = \widehat{\mathcal{S}} \setminus \{\mathcal{E}\} \cup \{\mathcal{E} \cup \{C\}\}$ // Add C to $\mathcal{E}$
25:         **else**
26:             $\widehat{\mathcal{S}} = \widehat{\mathcal{S}} \cup \{\{C\}\}$ // Create a new ECC for C
27:     **return** $\widehat{\mathcal{S}}$

represent the same circuit; e.g. the U2 and X instructions above can be swapped. RepGen eliminates some of this representation redundancy by the same mechanism it uses for avoiding redundancy due to circuit equivalence.

We use $|L|$, DropFirst(L), and DropLast(L) to denote the number of gates in a circuit L, its suffix with $|L| - 1$ gates, and its prefix with $|L| - 1$ gates. Note that each of the latter two represents a subcircuit.

We fix an arbitrary total order over single-gate circuits (i.e., $C^{(1,q)}$), and lift it to a total order of circuits (i.e., sequences).

Definition 3 (Circuit Precedence). *We say L_1 precedes L_2, written $L_1 \prec L_2$, if $|L_1| < |L_2|$, or if $|L_1| = |L_2|$ and L_1 is lexicographically smaller than L_2.*

Algorithm 1 lists the RepGen algorithm, which proceeds in rounds and maintains a database $\mathcal{D}$ of circuits grouped by fingerprints (defined below), a (j, q)-complete ECC set $\mathcal{S}_j$, and a *representative set* (set of representatives) $\mathcal{R}_j$ for ECCs in $\mathcal{S}_j$. The j-th round produces a (j, q)-complete ECC set from the $(j - 1, q)$-complete ECC set generated in the previous round. Each round proceeds in two steps.

Step 1: Constructing circuits. Before the first round, the initial ECC set is $\mathcal{S}_0 = \emptyset$ and the representative set is $\mathcal{R}_0 = \{()\}$, i.e., a singleton set consisting of the empty circuit (over q qubits). In the j-th round, RepGen uses the

$(j-1, q)$-complete ECC set $\mathcal{S}_{j-1}$ and its representative set $\mathcal{R}_{j-1}$ computed previously, and constructs possible size-j circuits by appending a single gate to each circuit in $\mathcal{R}_{j-1}$ with size $j - 1$. RepGen enumerates all possible gates g and arguments ι according to $\mathcal{G}$ and Σ. For each generated circuit L', RepGen checks if DropFirst(L') is a representative from the previous round. If so, RepGen concludes that L' extends existing representatives and must be considered in generating $\mathcal{S}_j$. Otherwise, circuit L' is considered redundant and ignored. We prove the correctness of RepGen in Theorem 2.

To identify potentially equivalent circuits, RepGen computes circuit *fingerprints*, and uses them as keys for storing circuits in the hash table $\mathcal{D}$. The fingerprint is computed using fixed, randomly selected parameter values and quantum states. Recall that for a circuit C over q qubits and m parameters, and parameter values $\vec{p} \in \mathbb{R}^m$, $[\![C]\!](\vec{p})$ is a (concrete) $2^q \times 2^q$ complex matrix. The fingerprint of a circuit C is

$$\text{FingerPrint}(C) = \left| \langle\psi_0| [\![C]\!](\vec{p}_0) |\psi_1\rangle \right|, \qquad (3)$$

where the parameter values $\vec{p}_0$ and quantum states $|\psi_0\rangle$ and $|\psi_1\rangle$ are fixed and randomly selected, and $|\cdot|$ denotes modulus of a complex number. With infinite precision, eqs. (2) and (3) ensure that equivalent circuits have identical fingerprints. This section presents and analyzes RepGen assuming infinite precision, while Section 7.1 presents an adaptation for finite-precision floating-point arithmetic.

Step 2: Examining circuits with equal fingerprints. In Step 1, RepGen generates circuits and stores them in the hash table $\mathcal{D}$ grouped by their fingerprints. In Step 2, RepGen partitions each set $\gamma = \mathcal{D}[f]$ of potentially equivalent circuits into a verified ECC set using the function Eccify. Eccify considers each circuit in γ and checks if it is equivalent to some existing ECC in γ by querying the verifier (Section 4); the circuit is then either added to the matching ECC, or becomes a new singleton ECC. RepGen then combines the ECC sets for each γ to get the ECC set $\mathcal{S}_j$.

Having constructed an ECC set $\mathcal{S}_j$, RepGen computes $\mathcal{S}_j$'s representative set $\mathcal{R}_j$, which is the set of representatives of the ECCs in $\mathcal{S}_j$ (Algorithm 1 line 16). The representative of an ECC is its $\prec$-minimum circuit (Definition 3). During the operation of RepGen, singleton ECCs are important: their representatives must be considered when generating circuits in the next round, and they may grow to non-singleton ECCs as more circuits are generated. However, singleton ECCs in $\mathcal{S}_n$ ultimately yield no transformations, so we remove them from the result of the RepGen algorithm (line 17).

3.2 Correctness of RepGen

When constructing circuits of size j (in round j), RepGen only considers circuits L' that extend previously constructed representatives, i.e., DropLast(L') $\in \mathcal{R}_{j-1}$, and only when the extension leads to DropFirst(L') $\in \mathcal{R}_{j-1}$. In this section we prove that in spite of that, RepGen always generates

an (n, q)-complete ECC set. Below we use $\mathcal{D}_j$ to denote the value of $\mathcal{D}$ after Step 1 in RepGen's j-th round (i.e., at Algorithm 1 line 15) and $\mathcal{D}_0$ for the initial value of $\mathcal{D}$ (line 4).

Lemma 1. *Algorithm 1 maintains the following invariants (for any $1 \leq j \leq n$, and writing $\sqsubseteq$ for Hoare ordering, i.e., $\mathcal{X} \sqsubseteq \mathcal{Y} \equiv \forall X \in \mathcal{X}. \exists Y \in \mathcal{Y}. X \subseteq Y$):*

1. *$\mathcal{D}_{j-1} \sqsubseteq \mathcal{D}_j$, $\mathcal{S}_{j-1} \sqsubseteq \mathcal{S}_j$, and $\mathcal{R}_{j-1} \subseteq \mathcal{R}_j$;*
2. *for any $L \in C^{(n,q)}$, $L \in \bigcup \mathcal{D}_j$ iff $|L| \leq j$ and either $L = ()$ or $\text{DropFirst}(L), \text{DropLast}(L) \in \mathcal{R}_{j-1}$; and*
3. *for any $L \in C^{(n,q)}$, $L \in \mathcal{R}_j$ iff $|L| \leq j$ and L does not have a $\prec$-smaller equivalent circuit in $C^{(n,q)}$.*

Proof. For item 1, $\mathcal{D}_{j-1} \sqsubseteq \mathcal{D}_j$ and $\mathcal{S}_{j-1} \sqsubseteq \mathcal{S}_j$ follow from the monotonic updating of $\mathcal{D}$ (i.e., circuits are only added), and from monotonicity (w.r.t. Hoare ordering) of Eccify. To see that $\mathcal{R}_{j-1} \subseteq \mathcal{R}_j$, observe that in the j-th round, all circuits constructed are of size j, so any circuit added to an existing ECC has more gates than its representative in $\mathcal{R}_{j-1}$, which will therefore remain its representative in $\mathcal{R}_j$ (recall that if $|L| < |L'|$ then $L \prec L'$).

We prove item 2 by induction on j. Both the base case ($j = 1$) and the induction step follow from Algorithm 1 lines 9–13, combined with item 1 and either the definition of $\mathcal{D}_0$ or the induction hypothesis.

We prove item 3 by induction on j. Slightly generalizing from the statement above, we take the base case to be $j = 0$, which follows from line 5. In the induction step, for sufficiency, consider a circuit L, $1 \leq |L| \leq j$, with no $\prec$-smaller equivalent circuit. (The $|L| = 0$ case follows from line 5 and item 1.) Both $\text{DropFirst}(L)$ and $\text{DropLast}(L)$ are of size $\leq j - 1$ with no $\prec$-smaller equivalent circuits (if either had a $\prec$-smaller equivalent circuit, we could use it to construct a $\prec$-smaller equivalent circuit for L). By the induction hypothesis, $\text{DropFirst}(L), \text{DropLast}(L) \in \mathcal{R}_{j-1}$, so by item 2, $L \in \bigcup \mathcal{D}_j$. By lines 15–16, $\mathcal{R}_j$ includes the $\prec$-minimal element of each class of equivalent circuits in $\bigcup \mathcal{D}$, so it must include L. Necessity follows from sufficiency, combined with the fact that two circuits in $\mathcal{R}_j$ cannot be equivalent and that $\mathcal{R}_j$ does not contain circuits of size greater than j. $\square$

Theorem 2 (RepGen). *In Algorithm 1, every $\mathcal{S}_j$ ($0 \leq j \leq n$) is a (j, q)-complete ECC set, and the algorithm returns an (n, q)-complete ECC set.*

Proof. We proceed using proof by contradiction. Let j be the smallest such that $\mathcal{S}_j$ is not (j, q)-complete. We must have $j > 0$, with $\mathcal{S}_{j-1}$ $(j-1, q)$-complete, and by Lemma 1 item 1 $\mathcal{S}_j$ is also $(j-1, q)$-complete. (As $\mathcal{S}_{j-1} \sqsubseteq \mathcal{S}_j$, $\mathcal{S}_j$ only includes more transformations.) Let (L, L') be the minimal (under the pairwise lexicographic lifting of $\prec$) pair of equivalent circuits of size $\leq j$ that cannot be rewritten to each other using transformations included in $\mathcal{S}_j$. We must have $|L'| = j$, since otherwise $|L|, |L'| \leq j - 1$, but $\mathcal{S}_j$ is $(j-1, q)$-complete.

If $\text{DropFirst}(L')$ has a $\prec$-smaller equivalent circuit, then $\mathcal{S}_j$ can rewrite L' to a $\prec$-smaller equivalent circuit, which

it must also not be able to rewrite to L, contradicting the minimality of L'. Therefore, $\text{DropFirst}(L')$ does not have a $\prec$-smaller equivalent circuit; The same argument works for $\text{DropLast}(L')$. Therefore, by using Lemma 1 item 3 we get $\text{DropFirst}(L'), \text{DropLast}(L') \in \mathcal{R}_{j-1}$, and by Lemma 1 item 2, $L' \in \mathcal{D}_j$. But if $L' \in \mathcal{D}_j$ then either $\mathcal{S}_j$ includes a transformation that rewrites L' to a smaller equivalent circuits, that it cannot rewrite to L, contradicting the minimality of L'; or L' does not have a $\prec$-smaller equivalent circuit, contradicting the definition of the pair (L, L'). $\square$

3.3 Complexity of RepGen

We analyze the time complexity of RepGen (its space complexity is the same). First, observe that the number of single-gate circuits $|C^{(1,q)}| - 1$, which is determined by the gate set $\mathcal{G}$, parameter-expression specification Σ, number of qubits q, and parameters m, provides an upper bound for the number of single-gate extensions of any existing circuit. (The -1 is due to $() \in C^{(1,q)}$.) This *characteristic* of $\mathcal{G}$, Σ, q, and m, denoted $\text{ch}(\mathcal{G}, \Sigma, q, m) = |C^{(1,q)}| - 1$, bounds the number of iterations of the loops in Algorithm 1 lines 10 and 11 in each round. (The bound may not be tight as Σ may impose more restrictions, e.g., single use of parameters.)

While $\sum_{j=0}^{n} \text{ch}(\mathcal{G}, \Sigma, q, m)^j$ provides a trivial upper bound on the complexity of RepGen, the following theorem shows that RepGen's running time can be bounded using the number of *resulting representatives* $|\mathcal{R}_n|$. In practice, this number is significantly smaller than $\text{ch}(\mathcal{G}, \Sigma, q, m)^n$ (see Table 5).

Theorem 3 (Complexity of RepGen). *The time complexity of Algorithm 1, excluding the verification part (line 15), is*

$$O\big(|\mathcal{R}_n| \cdot \text{ch}(\mathcal{G}, \Sigma, q, m) \cdot n\big).$$

Proof. The j-th round of Algorithm 1 considers circuits from $\mathcal{R}_{j-1}$ with size $j - 1$, and for each one it considers at most $\text{ch}(\mathcal{G}, \Sigma, q, m)$ possible extensions. It takes $O(n)$ to construct a new circuit and add it to $\mathcal{D}$. (We assume $O(1)$ complexity for hash table insert and lookup, i.e., we use average and amortized complexity.) Summing over all rounds of Algorithm 1, and recalling that $\mathcal{R}_j \subseteq \mathcal{R}_n$ (Lemma 1 item 1):

$$\sum_{j=1}^{n} |\{L \in \mathcal{R}_{j-1} : |L| = j - 1\}| \cdot \text{ch}(\mathcal{G}, \Sigma, q, m) \cdot n$$
$$\leq |\mathcal{R}_n| \cdot \text{ch}(\mathcal{G}, \Sigma, q, m) \cdot n.$$

$\square$

Note that if $\mathcal{G}$, Σ, q, and m are considered as constant then the time complexity of Algorithm 1 is $O(|\mathcal{R}_n| \cdot n)$.

Table 5 lists some empirical $\text{ch}(\mathcal{G}, \Sigma, q, m)$ and $|\mathcal{R}_n|$ values.

4 Circuit Equivalence Verifier

Given two circuits C_1 and C_2 over q qubits and m parameters, the verifier checks if they are equivalent (i.e., up to a global phase). Recalling eq. (2), that means checking if

$\forall \vec{p} \in \mathbb{R}^m. \ \exists \beta \in \mathbb{R}. \ [\![C_1]\!](\vec{p}) = e^{i\beta}[\![C_2]\!](\vec{p})$. Note that the equality here is between two $2^q \times 2^q$ complex matrices.

There are two challenges in automatically checking eq. (2). One is the quantifier alternation, which may be needed to account for global phase; the other is the use of trigonometric function, which is common in quantum gates' matrix representations. For example, the U_3 gate supported by the IBM quantum processors has the following matrix representation:

$$[\![U_3]\!](\theta, \phi, \lambda) = \begin{pmatrix} \cos\left(\frac{\theta}{2}\right) & -e^{i\lambda}\sin\left(\frac{\theta}{2}\right) \\ e^{i\phi}\sin\left(\frac{\theta}{2}\right) & e^{i(\phi+\lambda)}\cos\left(\frac{\theta}{2}\right) \end{pmatrix}. \quad (4)$$

While some SMT solvers support quantifiers and trigonometric functions [8, 9], our preliminary attempts showed they cannot directly prove eq. (2) for the circuit transformations generated by Quartz. Our verification approach is therefore to reduce eq. (2) to a quantifier-free formula over nonlinear real arithmetic by eliminating both the quantification over β and the trigonometric functions. The resulting verification conditions are then checked using the Z3 [10] SMT solver. This approach can efficiently verify all circuit transformations generated in our experiments (Section 7.4).

Phase factors. To eliminate the existential quantification over the phase β, we search over a finite space of linear combinations of the parameters $\vec{p}$ for a value that can be used for β. We consider $\beta(\vec{p}) = \vec{a} \cdot \vec{p} + b$, where $\vec{a} \in A$ and $b \in B$ for some *finite* sets $A \subseteq \mathbb{R}^m$ and $B \subseteq \mathbb{R}$. (Our experimentation with various combinations of quantum gates suggested that $\vec{a} \neq \vec{0}$ is sometimes needed, so we develop the mechanism with this generality; however, in the experiments reported in Section 7, constant phase factors, i.e. $\vec{a} = \vec{0}$, turned out to be sufficient for the three gate sets and the parameter specifications used.) Given circuits C_1 and C_2, we find candidates for the coefficients $\vec{a}$ and b using an approach similar to the one we use for generating candidate transformations. We select random parameter values $\vec{p}_0$ and quantum states $|\psi_0\rangle$ and $|\psi_1\rangle$ and find all combinations of $\vec{a}$ and b as above that satisfy the following equation up to a small floating-point error (note that unlike eq. (3), $|\cdot|$ is not used):

$$\langle\psi_0|\,[\![C_1]\!](\vec{p}_0)\,|\psi_1\rangle = e^{i(\vec{a}\cdot\vec{p}+b)} \cdot \langle\psi_0|\,[\![C_2]\!](\vec{p}_0)\,|\psi_1\rangle, \quad (5)$$

For every such candidate coefficients $\vec{a}$ and b, we then attempt to verify following equation,

$$\forall \vec{p} \in \mathbb{R}^m. \ [\![C_1]\!](\vec{p}) = e^{i(\vec{a}\cdot\vec{p}+b)}[\![C_2]\!](\vec{p}), \quad (6)$$

which unlike eq. (2), does not existentially quantify over β. If eq. (6) holds for some candidate coefficients, then C_1 and C_2 are verified to be equivalent. Otherwise, we consider the transformation given by C_1 and C_2 to fail verification, but that case did not occur in our experiments.

Trigonometric functions. Matrices of parametric quantum gates we encountered only use their parameters inside arguments to sin or cos (after applying Euler's formula).

(a) A circuit transformation.

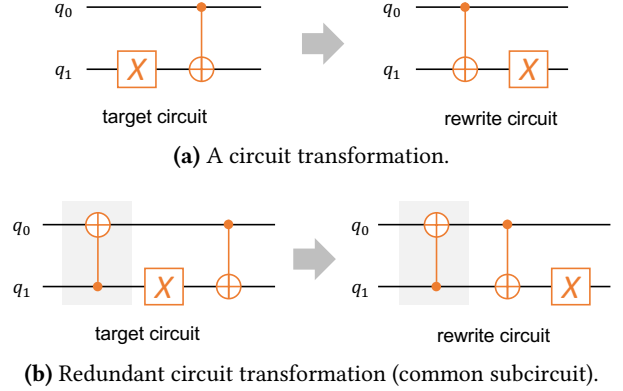**(b)** Redundant circuit transformation (common subcircuit).

Figure 4. Illustrating a redundant circuit transformation.

Under this assumption, we reduce eq. (6) to nonlinear real arithmetic in three steps. First, we eliminate expressions such as $\frac{\theta}{2}$ that occur in some quantum gates (e.g., eq. (4)) by introducing a fresh variable $\theta' = \frac{\theta}{2}$ and substituting $\theta' + \theta'$ for θ. After this step, all arguments to sin and cos are linear combinations of variables and constants (e.g., from phase factors) with integer coefficients. Second, we exhaustively apply Euler's formula $e^{i\phi} = \cos\phi + i\sin\phi$, and trigonometric identities for parity and sum of angles: $\sin(-x) = -\sin(x)$, $\cos(-x) = \cos(x)$, $\sin(x + y) = \sin(x)\cos(y)+\cos(x)\sin(y)$, and $\cos(x + y) = \cos(x)\cos(y) - \sin(x)\sin(y)$. After these steps, sin and cos are only applied to atomic terms (variables and constants). For each constant c, we require precise symbolic expressions for $\sin(c)$ and $\cos(c)$ (e.g., $\sin(\frac{\pi}{4}) = \frac{\sqrt{2}}{2}$), and eliminate sin and cos over constants using these expressions. Third, for every variable t such that $\sin(t)$ or $\cos(t)$ is used we substitute s_t for $\sin(t)$ and c_t for $\cos(t)$, where s_t and c_t are fresh variables with a constraint $s_t^2 + c_t^2 = 1$, which fully eliminates trigonometric functions.

Ultimately, Z3 can check the transformed version of eq. (6) using the theory of quantifier-free nonlinear real arithmetic.

During the development of Quartz we occasionally encountered verification failures, but these were due to implementation bugs, and the counterexamples obtained from Z3 were useful in the debugging process. Thus, verification is useful not only to ensure the ultimate correctness of the generated transformations, but also in the development process.

5 Pruning Redundant Transformations

Quartz applies two pruning steps after RepGen generates an (n, q)-complete ECC set to further eliminate redundancy. These steps maintain (n, q)-completeness while reducing the number of transformations the optimizer needs to consider.

5.1 ECC Simplification

All ECCs generated by RepGen have circuits with exactly q qubits. For each ECC, a qubit (or a parameter) is *unused* if all circuits in the ECC do not operate on the qubit (or the

parameter). An *ECC simplification* pass removes all unused qubits and parameters from each ECC. After this pass, some ECCs may become identical, among which only one is kept.

Because there is no specific order on parameters in a circuit, Quartz also finds identical ECCs under a permutation of the parameters and maintains only one of them.

5.2 Common Subcircuit Pruning

Quartz eliminates transformations whose target and rewrite circuits include a common subcircuit at the beginning or the end. Figure 4 illustrates this *common subcircuit pruning*; the common subcircuit is highlighted in grey. Theorem 4 explains why such transformations are always redundant.

Definition 4. *A subset of gates C' in a circuit C is a* subcircuit at the beginning *of C if all gates in C' are topologically before all gates in $C \setminus C'$. Similarly, a subset of gates C' in a circuit C is a* subcircuit at the end *of C if all gates in C' are topologically after all gates in $C \setminus C'$.*

Theorem 4. *For any two quantum circuits C_1 and C_2 with a common subcircuit at the beginning or the end, if C_1 and C_2 are equivalent, then eliminating the common subcircuit from C_1 and C_2 generates two equivalent circuits.*

Proof. Recall that $[\![C]\!](\vec{p})$ (for all $\vec{p}$—we elide $\vec{p}$ in this proof) denotes the matrix representation of circuit C. Let $[\![C]\!]^\dagger$ be the conjugate transpose of $[\![C]\!]$, and recall that as $[\![C]\!]$ is unitary, we have $[\![C]\!]^\dagger [\![C]\!] = [\![C]\!][\![C]\!]^\dagger = I$. Let C_s denote the common subcircuit shared by C_1 and C_2. Let C_1' and C_2' represent the new circuits obtained by removing C_s from C_1 and C_2. When C_s is a common subcircuit at the beginning of C_1 and C_2, the matrix representations for the new circuits are $[\![C_i']\!] = [\![C_s]\!]^\dagger [\![C_i]\!]$, where $i = 1, 2$. Equivalence between C_1 and C_2 implies the existence of β such that $[\![C_1]\!] = e^{i\beta}[\![C_2]\!]$, therefore $[\![C_1']\!] = e^{i\beta}[\![C_2']\!]$. The case where C_s is a common subcircuit at the end is similar. $\square$

Theorem 4 shows that every transformation pruned in common subcircuit pruning must be subsumed by other transformations (assuming initial (n, q)-completeness).

Observe that if two circuits have a common subcircuit at the beginning (resp. the end), then they must have a common gate at the beginning (resp. the end). Therefore, to implement common subcircuit pruning, Quartz only checks for a single common gate at the beginning or the end.

6 Circuit Optimizer

Quartz's *circuit optimizer* applies the verified transformations generated by the generator to find an optimized equivalent circuit for a given input circuit (see Figure 1).

A key step is computing $\text{Apply}(C, T)$, the set of circuits that can be obtained by applying transformation $T = (C_T, C_R)$ to circuit C. This involves finding all possible ways to match C_T with a subcircuit of C. Quartz's optimizer uses a *graph representation for circuits*, explained below, to implement
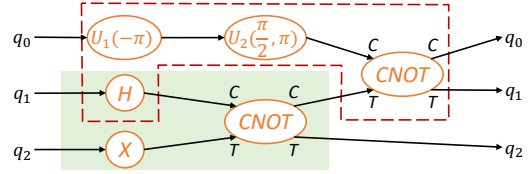

Figure 5. Graph representation for Figure 2a's circuit. The green box (subcircuit, also convex subgraph) and red dashed area (not a subcircuit, also non-convex subgraph) match those of Figure 2a.

this operation. In the graph representation, subcircuits correspond to convex subgraphs,[1] and Quartz adapts the graph-matching procedure from TASO [17] to find all matches between C_T and a convex subgraph of C.

In the graph representation, a circuit C over q qubits is represented as a directed graph G, where each gate over d qubits is a vertex with in- and out-degree d. Edges are labeled to distinguish between qubits in multi-qubit gates (e.g., the control and target qubits of a $CNOT$ gate). G also includes q sources and sinks, one for each qubit. Figure 5 illustrates the graph representation of Figure 2a's circuit. As the figure also illustrates, subcircuits correspond to convex subgraphs.

The optimizer first converts an (n, q)-complete ECC set into a set of transformations (in the graph representation). For each ECC with x equivalent circuits $C_1, \ldots, C_x$, the optimizer considers a pair of transformations between the representative and each other circuit. For example, if C_1 is the representative circuit in the ECC, then the optimizer considers transformations $C_1 \rightarrow C_i$ and $C_i \rightarrow C_1$ for $1 < i \leq x$. These $2(x - 1)$ transformations guarantee that any two circuits from the same ECC are reachable from each other.

To optimize an input circuit using the above transformations, the optimizer uses a *cost-based backtracking search* algorithm adapted from TASO [17, 18]. The search is guided by a cost function $\text{Cost}(\cdot)$ that maps circuits to real numbers. In our evaluation, the cost is given by the number of gates in a circuit, but other cost functions are possible.

Algorithm 2 shows the pseudocode of our search algorithm. To find an optimized circuit, candidate circuits are maintained in a priority queue Q. At each iteration, the lowest-cost circuit C is dequeued, and Quartz applies all transformations to get equivalent new circuits C_{new}, which are enqueued into Q for further exploration. Circuits considered in the past are ignored using $\mathcal{D}_{seen}$.

The search is controlled by a hyper-parameter γ. Quartz ignores candidate circuits whose cost is greater than γ times the cost of the current best circuit C_{best}. The parameter γ trades off between search time and the search's ability to avoid local minima. For $\gamma = 1$, Algorithm 2 becomes a greedy

---

[1]For a graph G, G' is a convex subgraph of G if for any two vertices u and v in G', every path in G from u to v is also contained in G'.
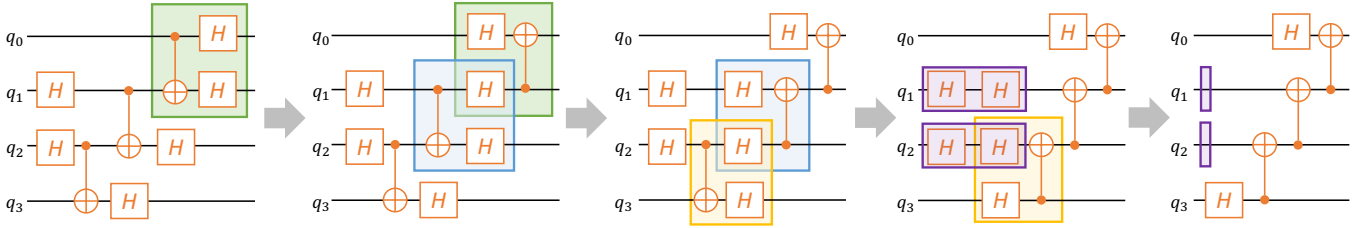
Figure 6. A transformation sequence applied by Quartz that reduces the total gate count in the `gf2^4_mult` circuit by swapping the control and target qubits of three *CNOT* gates. Note that the first three transformations do not reduce gate count.

Algorithm 2 Cost-Based Backtracking Search Algorithm.

1: **Inputs:** Verified transformations $\mathcal{T}$, a cost model $\text{Cost}(\cdot)$, a hyper-parameter γ, and an input circuit C_{in}.
2: **Output:** an optimized circuit C_{best}
3: // Q is a priority queue of circuits sorted by their $\text{Cost}(\cdot)$.
4: $Q = \{C_{in}\}$
5: $C_{best} = C_{in}$
6: $\mathcal{D}_{seen} = \{C_{in}\}$
7: **while** $Q \neq \emptyset$ and the search has not timed out **do**
8:     $C = Q.\text{dequeue}()$
9:     **if** $\text{Cost}(C) < \text{Cost}(C_{best})$ **then**
10:         $C_{best} = C$
11:     **for** each transformation $T \in \mathcal{T}$ **do**
12:         **for** each $C_{new} \in \text{Apply}(C, T) \setminus \mathcal{D}_{seen}$ **do**
13:             **if** $\text{Cost}(C_{new}) < \gamma \cdot \text{Cost}(C_{best})$ **then**
14:                 $Q.\text{enqueue}(C_{new})$
15:                 $\mathcal{D}_{seen} = \mathcal{D}_{seen} \cup \{C_{new}\}$
16: **return** C_{best}

Table 1. Gate sets used in our evaluation.

Name	Supported Gates
Nam [15, 23]	H, X, $R_z(\lambda)$, $CNOT$
IBM [12]	$U_1(\theta)$, $U_2(\phi, \lambda)$, $U_3(\theta, \phi, \lambda)$, $CNOT$
Rigetti [26]	$R_x(\frac{\pi}{2})$, $R_x(-\frac{\pi}{2})$, $R_x(\pi) = X$, $R_z(\lambda)$, CZ

7 Implementation and Evaluation

We describe our implementation of Quartz and evaluate the performance of the generator, the verifier, and the optimizer. Quartz is publicly available as an open-source project [4] and also in the artifact supporting this paper [32].

7.1 Implementation

Floating-point arithmetic. The RepGen algorithm as presented in Section 3 uses real-valued fingerprints, where two equivalent circuits always have the same fingerprint. Our implementation of RepGen uses floating-point arithmetic, which introduces some imprecision that can potentially lead to different fingerprints for equivalent circuits. To account for this imprecision, the implementation assumes there exists an *absolute error threshold* E_{max}, such that fingerprints of equivalent circuits differ by at most E_{max} when computed with floating-point arithmetic. The implementation therefore computes, using floating-point arithmetic, the integer $\left\lfloor \frac{\text{FingerPrint}(C)}{2E_{max}} \right\rfloor$, and uses it as the key for storing circuit C in $\mathcal{D}$. Under our assumption, equivalent circuits may still have different integer hash keys, but they may differ only by 1. Therefore, the implementation introduces an additional step after line 15 of Algorithm 1, in which ECCs that correspond to circuits with hash keys h and $h + 1$ are checked for equivalence and merged if found equivalent. In our experiments we set $E_{max} = 10^{-15}$ based on preliminary exploration of the floating-point errors that occur in practice.

Supported gate sets. Quartz is a generic quantum circuit optimizer supporting arbitrary gate sets, and it accepts a gate set $\mathcal{G}$ as part of its input. In our experiments, input circuits are given over the "Clifford + T" gate set: H, T, $T^\dagger$, S, $S^\dagger$, and $CNOT$; and output (optimized) circuits are in one of the three gate sets listed in Table 1: Nam, IBM, and Rigetti. Nam is a

search that only accepts transformations that strictly improve cost. On the other hand, a higher value for γ enables application of transformations that do not immediately improve the cost, which may later lead to otherwise inaccessible optimization opportunities. For example, Figure 6 depicts a sequence of five transformations that reduce the total gate count in the `gf2^4_mult` (see Section 7.3) circuit by four, via flipping three *CNOT* gates; note that the first three transformations do not reduce the gate count at all.

Quartz's circuit optimizer is designed to optimize circuits before *mapping*. *Circuit mapping* converts a quantum circuit to an equivalent circuit that satisfies hardware constraints of a given quantum processor. These constraints include connectivity restrictions between qubits and the directions to perform multi-qubit operations. While transformations discovered by Quartz are also applicable to circuits after mapping, applying them naively may break hardware constraints. Therefore, we leave it as future work to build an optimizer for after-mapping circuits using Quartz's transformations.

gate set commonly used in prior work [15, 23], IBM is derived from the IBMQX5 quantum processor [12], and Rigetti is derived from the Rigetti Agave quantum processor [3, 26].

To generate and verify circuit transformations for a new gate set, Quartz only requires, for each gate, a specification of its matrix representation as a function of its parameters, such as eq. (1). To optimize circuits, a translation procedure of input circuits to the new gate set is also required unless input circuits are provided in the new gate set.

Rotation merging and Toffoli decomposition. Before invoking Quartz's optimizer, Quartz preprocesses circuits by applying two optimizations: *rotation merging* and *Toffoli decomposition* [23]. Our preliminary experiments showed that an approach solely based on local transformations and a cost-based search cannot reproduce these optimization passes for large circuits. Rotation merging combines multiple R_z/U_1 gates that may be arbitrarily far apart (separated by X or $CNOT$ gates), and appears difficult to be represented as local circuit transformations. Toffoli decomposition decomposes a Toffoli gate into the Nam gate set, which involves simultaneous transformation of 15 quantum gates and interacts with rotation merging [23, p. 11]. We therefore implement these two optimization passes from prior work [23] as a pre-processing step. Toffoli decomposition requires selecting a polarity for each Toffoli gate, which is computed heuristically by prior work [23]. Instead, we use a greedy approach: we process the Toffoli gates sequentially and for each gate we consider both polarities and greedily pick the one that results in fewer gates after rotation merging.

For the Nam and IBM gate sets, Quartz directly applies rotation merging and Toffoli decomposition as a preprocessing step before the optimizer. For the Rigetti gate set, which includes CZ rather than $CNOT$, the algorithm from the prior work [23] is not directly applicable; therefore, Quartz uses several additional preprocessing steps, as follows. Rather than directly transpiling an input circuit to Rigetti, Quartz first transpiles it to Nam and applies Toffoli decomposition and rotation merging. Next, Quartz rewrites each $CNOT$ gate to a sequence of H, CZ, H gates, cancels out adjacent H or CZ pairs, and then fully converts the circuit to Rigetti by transforming X to $R_x(\pi)$ and H to $R_x(\pi) \cdot R_z(\frac{\pi}{2}) \cdot R_x(\frac{\pi}{2}) \cdot R_z(-\frac{\pi}{2})$. Ultimately, Quartz invokes the optimizer, using a suitable (n, q)-complete ECC set for Rigetti. Note that elimination of adjacent H or CZ pairs during the translation from Nam to Rigetti leads to more optimized circuits: a pair of adjacent H gates (that are canceled out) would otherwise be transformed into a sequence of eight R_x and R_z gates that cannot be canceled out by Quartz since the cancellation is only correct for specific parameter values, while Quartz considers symbolic transformations valid for arbitrary parameter values.

Symbolic parameter expressions. As explained in Section 2, Quartz assumes a fixed number of parameters m and a specification Σ for parameter expressions used in circuits.

Quartz takes m as input, and supports a flexible form for Σ defined by a finite set of parameter expressions and either allowing or disallowing parameters to be used more than once in a circuit.

Our experiments use $m = 2$ for the Nam and Rigetti gate sets, and $m = 4$ for the IBM gate set because it contains gates with up to three parameters. For Σ, we consider the expressions p_i, $2p_i$ and $p_i + p_j$ where $0 \le i < m$ and $i < j < m$ (recall that $\vec{p} \in \mathbb{R}^m$ is the vector of parameters), and restrict each parameter to be used at most once in a circuit. This restriction significantly reduces the number of circuits RepGen considers, especially for the IBM gate set because the U_3 gate requires three parameter expressions.

As explained in Section 4, the verifier searches for phase factors of the form $\vec{a} \cdot \vec{p} + b$. In our experiments we used $a \in \{-2, -1, 0, 1, 2\}^m$ and $b \in \{0, \frac{\pi}{4}, \frac{2\pi}{4}, \ldots, \frac{7\pi}{4}\}$, which proved to be useful and sufficient in our preliminary experimentation with various gates. We later found that for the gate sets of Table 1, $\vec{a} = \vec{0}$ is actually sufficient. That is, these gate sets do not admit any transformations with parameter-dependent phase factors for the circuits we considered; they do however need various constant phase factors.

7.2 Experiment Setup

We compare Quartz with existing quantum circuit optimizers on a benchmark suite of 26 circuits developed by prior work [6, 23]. The benchmarks include arithmetic circuits (e.g., adding integers), multiple controlled X and Z gates (e.g., CCX and CCZ), the Galois field multiplier circuits, and quantum Fourier transformations. We use Quartz to optimize the benchmark circuits to the three gate sets of Table 1.

As in prior work [15, 23], we measure cost of a circuit in terms of the total gate count. We therefore define the Cost function in Algorithm 2 as the number of gates in a circuit.[2]

Setting n and q for generating an (n, q)-complete ECC set determines the resulting transformations. Our experiments use: $n = 6$, $q = 3$ for the Nam gate set; $n = 4$, $q = 3$ for the IBM gate set; and $n = 3$, $q = 3$ for the Rigetti gate set, which provided good results for our benchmarks. Sections 7.4 and 7.5 discuss the impact of n and q on Quartz's performance.

Quartz's backtracking search (Algorithm 2) is controlled by the hyper-parameter γ and the timeout threshold. Our experiments use $\gamma = 1.0001$, which yields good results for our benchmarks. This value for γ essentially means we consider cost-preserving transformations but not cost-increasing ones. For the search timeout, we use 24 hours. Section 7.5 discusses the timeout threshold and how it interacts with the settings for n and q. To stop the search from consuming too much memory, whenever the priority queue of Algorithm 2 contains more than 2,000 circuits we prune it and keep only the

---

[2]Quartz can in principle be used to optimize for other metrics, e.g. number of $CNOT$ or T gates, but here we focus on total gate count.

Table 2. Gate count results for the Nam gate set. The best result for each circuit is in bold. "Quartz Preprocess" lists gate count after Quartz's preprocessor (Section 7.1).

Circuit	Orig.	Qiskit	Nam	voqc	Quartz Preprocess	Quartz End-to-end
adder_8	900	869	**606**	682	732	724
barenco_tof_3	58	56	40	50	46	**38**
barenco_tof_4	114	109	72	95	86	**68**
barenco_tof_5	170	162	104	140	126	**98**
barenco_tof_10	450	427	264	365	326	**262**
csla_mux_3	170	168	155	158	164	**154**
csum_mux_9	420	420	**266**	308	308	272
gf2^4_mult	225	213	187	192	186	**177**
gf2^5_mult	347	327	296	291	287	**277**
gf2^6_mult	495	465	403	410	401	**391**
gf2^7_mult	669	627	555	549	543	**531**
gf2^8_mult	883	819	712	705	**703**	**703**
gf2^9_mult	1095	1023	891	885	879	**873**
gf2^10_mult	1347	1257	1070	1084	1062	**1060**
mod5_4	63	62	51	56	51	**26**[†]
mod_mult_55	119	117	91	**90**	105	93
mod_red_21	278	261	**180**	214	236	202
qcla_adder_10	521	512	**399**	438	450	422
qcla_com_7	443	428	**284**	314	349	292
qcla_mod_7	884	853	-[††]	723	727	**719**
rc_adder_6	200	195	**140**	157	174	154
tof_3	45	44	**35**	40	39	**35**
tof_4	75	73	**55**	65	63	**55**
tof_5	105	102	**75**	90	87	**75**
tof_10	255	247	**175**	215	207	**175**
vbe_adder_3	150	146	89	101	115	**85**
Geo. Mean Reduction	-	3.9%	27.3%	18.7%	18.6%	28.7%

[†] Computed as the median of seven runs: 25, 26, 26, 26, 32, 32, 32.

[††] Nam generates an incorrect circuit for qcla_mod_7 [19, Table 1].

top 1,000 circuits. Our preliminary experimentation with this pruning suggested that it does not affect Quartz's results.

All experiments were performed on an m6i.32xlarge AWS EC2 instance with a 128-core CPU and 512 GB RAM.

7.3 Circuit Optimization Results

Nam gate set. Table 2 compares Quartz to Qiskit [5], Nam [23], and voqc [15] for the Nam gate set. (The performance of t|ket⟩ [28] for this gate set is similar to Qiskit, see [15].) The table also shows the gate count following Quartz's preprocessing steps (rotation merging and Toffoli decomposition, see Section 7.1). Quartz outperforms Qiskit and voqc on almost all circuits, indicating that it discovers most transformations used in these optimizers and also explores new optimization opportunities arising from new transformations and from the use of a cost-guided backtracking search (rather than a greedy approach, e.g., see Figure 6).

Quartz achieves on-par performance with Nam [23], a circuit optimizer highly tuned for this gate set. Nam applies a set of carefully chosen heuristics such as floating R_z gates

Table 3. Gate count results for the IBM gate set. The best result for each circuit is in bold. "Quartz Preprocess" lists gate count after Quartz's preprocessor (Section 7.1).

Circuit	Orig.	Qiskit	t|ket⟩	voqc	Quartz Preprocess	Quartz End-to-end
adder_8	900	805	775	643	736	**583**
barenco_tof_3	58	51	51	46	46	**36**
barenco_tof_4	114	100	100	89	86	**67**
barenco_tof_5	170	149	149	135	126	**98**
barenco_tof_10	450	394	394	347	326	**253**
csla_mux_3	170	153	155	148	164	**139**
csum_mux_9	420	382	361	**308**	364	340
gf2^4_mult	225	206	206	190	186	**178**
gf2^5_mult	347	318	319	289	287	**275**
gf2^6_mult	495	454	454	408	401	**388**
gf2^7_mult	669	614	614	547	543	**530**
gf2^8_mult	883	804	806	703	703	**692**
gf2^9_mult	1095	1006	1009	882	879	**866**
gf2^10_mult	1347	1238	1240	1080	1062	**1050**
mod5_4	63	58	58	53	55	**51**
mod_mult_55	119	106	102	**83**	109	91
mod_red_21	278	227	224	**191**	246	205
qcla_adder_10	521	460	460	409	450	**372**
qcla_com_7	443	392	392	292	349	**267**
qcla_mod_7	884	778	780	666	726	**594**
rc_adder_6	200	170	172	**141**	186	151
tof_3	45	40	40	36	39	**31**
tof_4	75	66	66	58	63	**49**
tof_5	105	92	92	80	87	**67**
tof_10	255	222	222	190	207	**157**
vbe_adder_3	150	133	139	100	115	**82**
Geo. Mean Reduction	-	11.0%	11.2%	23.1%	17.4%	30.1%

and canceling one- and two-qubit gates (see [23] for more detail). While Quartz's preprocessor implements two of Nam's optimization passes, the results of the preprocessor alone are not close to Nam.[3] By using the automatically generated transformations, Quartz is able to perform optimizations similar to some of Nam's other hand-tuned optimizations, and even outperform Nam on roughly half of the circuits.

For mod5_4, we observed significant variability between runs, caused by randomness in ordering circuits with the same cost in the priority queue (Q in Algorithm 2). Therefore, Table 2 reports the median result from seven runs as well as individual results. This variability also suggests that Quartz's performance can be improved by running the optimizer multiple times and taking the best discovered circuit, or by applying more advanced stochastic search techniques [21].

IBM gate set. Table 3 compares Quartz with Qiskit [5], t|ket⟩ [28], and voqc [15] on the IBM gate set. Qiskit and t|ket⟩ include a number of optimizations specific to this gate

---

[3]We observe that for the gf2^n_mult circuits, Quartz' preprocessor outperforms Nam. We attribute this difference to our greedy Toffoli decomposition, discussed in Section 7.1, which happens to work well for these circuits.

Table 4. Gate count results for the Rigetti gate set. The best result for each circuit is in bold. "Quartz Preprocess" lists gate count after Quartz's preprocessor (Section 7.1).

Circuit	Orig.	Quilc	t|ket⟩	Quartz Preprocess	Quartz End-to-end
adder_8	5324	3345	3726	4244	**2553**
barenco_tof_3	332	203	207	256	**148**
barenco_tof_4	656	390	408	500	**272**
barenco_tof_5	980	607	609	744	**386**
barenco_tof_10	2600	1552	1614	1964	**960**
csla_mux_3	1030	**614**	641	864	654
csum_mux_9	2296	1540	1542	1736	**1100**
gf2^4_mult	1315	809	827	1020	**796**
gf2^5_mult	2033	1301	1277	1573	**1231**
gf2^6_mult	2905	1797	1823	2235	**1751**
gf2^7_mult	3931	2427	2465	3021	**2371**
gf2^8_mult	5237	3208	3276	4033	**3081**
gf2^9_mult	6445	4070	4037	4933	**3986**
gf2^10_mult	7933	4977	**4967**	6048	5039
mod5_4	369	211	238	293	**197**
mod_mult_55	657	420	452	531	**361**
mod_red_21	1480	880	1020	1166	**738**
qcla_adder_10	3079	–[†]	1884	2464	**1615**
qcla_com_7	2512	1540	1606	1954	**1095**
qcla_mod_7	5130	3164	3202	4029	**2525**
rc_adder_6	1186	706	747	984	**606**
tof_3	255	150	160	201	**135**
tof_4	425	271	270	333	**199**
tof_5	595	354	380	465	**271**
tof_10	1445	878	930	1125	**631**
vbe_adder_3	900	534	557	705	**366**
Geo. Mean Reduction	-	38.6%	36.3%	21.9%	49.4%

[†] Quilc supports up to 32 qubits while qcla_adder_10 has 36.

set, such as merging any sequence of U_1, U_2, and U_3 gates into a single gate [2] and replacing any block of consecutive 1-qubit gates by a single U_3 gate [1]. Quartz is able to automatically discover some of these gate-specific optimizations by representing them each as a sequence of transformations. Overall, Quartz outperforms these existing compilers.

Rigetti gate set. Table 4 compares Quartz with Quilc [29] and t\|ket⟩ [28] on the Rigetti gate set. Quartz significantly outperforms t\|ket⟩ and Quilc on most circuits, even though Quilc is highly optimized for this gate set. We also note that while we employ some simplifications in the preprocessing phase for the Rigetti gate set (see Section 7.1), most of the reduction in gate count comes from the optimization phase.

7.4 Analyzing Quartz's Generator and Verifier

We now examine Quartz's circuit generator and circuit equivalence verifier. Table 5 shows the run times of the entire generation procedure, and also the time out of that spent in verification, for each of the three gate sets and for varying values of n, while fixing $q = 3$. The table also lists the

Table 5. Metrics for Quartz's generator, when generating (n, q)-complete ECC sets for $q=3$ and varying values of n for the three gate sets. $|\mathcal{T}|$ is the resulting number of transformations, $|\mathcal{R}_n|$ is the size of the resulting representative set, and ch is the characteristic (see Algorithm 1 and Theorem 3).

	n	$|\mathcal{T}|$	$|\mathcal{R}_n|$	Verification Time (s)	Total Time (s)
Nam ch = 27	2	62	397	1.2	1.3
	3	196	4,179	2.6	3.7
	4	1,304	36,177	8.5	21.4
	5	8,002	269,846	49.5	174.7
	6	56,152	1,777,219	370.3	1,400.4
	7	379,864	10,432,127	2,673.6	10,461.2
IBM ch = 1, 362	2	1,912	22,918	22.9	38.6
	3	5,086	224,281	100.4	225.9
	4	16,748	1,552,185	356.9	1,290.0
	5	225,068	7,847,203	1,844.8	8,363.1
Rigetti ch = 30	2	66	361	1.3	1.5
	3	66	3,143	2.6	3.7
	4	224	22,043	5.8	15.4
	5	2,396	134,423	22.7	100.2
	6	15,464	729,842	132.0	675.3

Table 6. Number of circuits considered when using REP-GEN with or without the pruning techniques of Section 5 to generate (n, q)-complete ECC sets for $q=3$ and varying values of n for the three gate sets. Circuits are counted by their sequence representation, as REPGEN considers multiple sequences for each actual circuit (Section 3). Parenthesis shows reduction relative to the number of all possible circuits for n and q. "REPGEN" corresponds to REPGEN without additional pruning. "+ ECC Simplification" corresponds to REPGEN combined with ECC simplification. "+ Common Subcircuit" corresponds to REPGEN combined with all pruning techniques and ultimately represents Quartz's generator.

	n	Possible Circuits	REPGEN	+ ECC Simplification	+ Common Subcircuit
Nam	2	604	400 (2×)	50 (12×)	50 (12×)
	3	11,404	1,180 (10×)	231 (49×)	164 (70×)
	4	198,028	5,178 (38×)	2,170 (91×)	1,199 (165×)
	5	3,246,220	31,517 (103×)	18,244 (178×)	7,661 (424×)
	6	51,021,964	195,466 (261×)	131,554 (388×)	54,538 (936×)
	7	776,616,076	1,196,163 (649×)	875,080 (887×)	369,973 (2,099×)
IBM	2	35,005	23,413 (1×)	1,708 (20×)	1,708 (20×)
	3	533,857	62,594 (9×)	10,287 (52×)	4,563 (117×)
	4	6,446,209	185,315 (35×)	65,343 (99×)	15,746 (409×)
	5	68,078,785	921,611 (74×)	512,975 (133×)	219,551 (310×)
Rigetti	2	778	469 (2×)	51 (15×)	51[†] (15×)
	3	17,518	965 (18×)	117 (150×)	51[†] (343×)
	4	367,843	2,293 (160×)	548 (671×)	203 (1,812×)
	5	7,354,093	10,568 (696×)	4,949 (1,486×)	2,337 (3,147×)
	6	141,763,468	58,193 (2,436×)	35,690 (3,972×)	15,240 (9,302×)

[†] For Rigetti, $n = 2$ and $n = 3$ result in identical transformations—each 3-gate transformation is subsumed by 2-gate transformations in a way identified by Quartz.

number of resulting circuit transformations $|\mathcal{T}|$, the size of the resulting representative set $|\mathcal{R}_n|$, and the characteristic (see Algorithm 1 and Theorem 3). For all gate sets, $|\mathcal{T}|$ and

$|\mathcal{R}_n|$ grow exponentially with n. In spite of this exponential growth, the generator and verifier can generate, in a reasonable run time of a few hours, an (n, q)-complete ECC set for values of n and q that are sufficiently large to be useful for circuit optimization. The growth in the number of transformations significantly affects the optimizer. For Nam and IBM, our selected values of $n = 6$ and $n = 4$ result in a similar order of magnitude for $|\mathcal{T}|$. For Rigetti, we use $n = 2$, resulting in much smaller $\mathcal{T}$. This choice is related to the fact that circuits in the Rigetti gate set are larger by roughly an order of magnitude compared to Nam and IBM (compare "Orig." in Table 4 with Tables 2 and 3; see discussion in Section 7.5).

We now evaluate the effectiveness of RepGen and the pruning techniques described in Section 5 for reducing the number of circuits Quartz must consider (which is closely correlated with the number of resulting transformations). To evaluate the relative contribution of each technique, Table 6 reports the number of circuits considered when applying: (i) RepGen without additional pruning, (ii) RepGen combined with ECC simplification, and (iii) RepGen combined with both ECC simplification and common subcircuit pruning; and compares each of these to a brute force approach of generating all possible circuits with up to q qubits and n gates. Both RepGen and the pruning techniques play an important role in eliminating redundant circuits while preserving (n, q)-completeness. Ultimately, RepGen and the pruning techniques reduce the number of transformations the optimizer must consider by one to three orders of magnitude.

7.5 Analyzing Quartz's Circuit Optimizer

We now examine Quartz's circuit optimizer when using an (n, q)-complete ECC set for varying values of n and q. For this study we focus on the Nam gate set, and compare different values for n and q by the *optimization effectiveness* they yield, defined as the reduction in geometric mean gate count over all circuits (as in the bottom line of Table 2). For mod5_4, when $q = 3$ and $3 \le n \le 7$, we use the median of 7 runs due to the variability discussed in Section 7.3.

As we increase n and q we expect Quartz's optimizer to: (i) be able to reach more optimized circuits, and (ii) require more time per search iteration. Both of these follow from the fact that increasing n and q yields more transformations. Under a fixed search time budget, we expect the increased cost of search iterations to reduce the positive impact of larger n's and q's. Because each iteration (Algorithm 2) considers a candidate circuit C and computes Apply(C, T) for each transformation $T \in \mathcal{T}$, the cost per iteration scales linearly with the number of transformations $|\mathcal{T}|$. Since $|\mathcal{T}|$ varies dramatically as n and q change,[4] we expect the second effect (slowing down the search) to be significant, especially for

[4]For example: with $q = 3$, $|\mathcal{T}| = 196$ for $n = 3$ and $|\mathcal{T}| = 56, 152$ for $n = 6$ (Table 5); with $q = 4$, $|\mathcal{T}| = 208$ for $n = 3$ and $|\mathcal{T}| = 273, 532$ for $n = 6$ [33]. We were unable to generate a $(7, 4)$-complete ECC set using 512 GB of RAM.
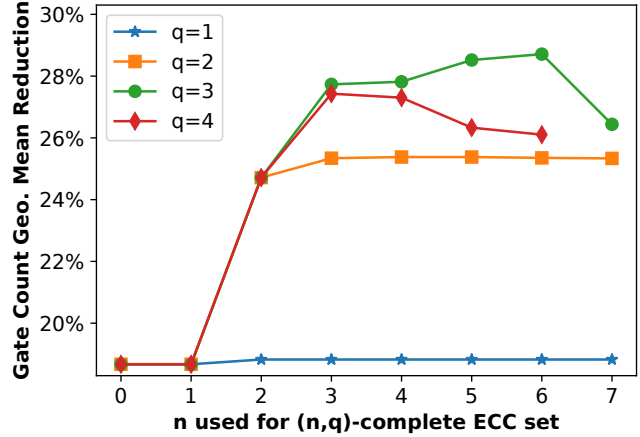

Figure 7. Optimization effectiveness with (n, q)-complete ECC sets for varying n and q after a 24-hour search timeout. For $n = 0$ there are no transformations and the results match the "Quartz Preprocess" column of Table 2.

large circuits which typically require more search iterations (and additionally increase Apply's running time).

Figure 7 shows optimization effectiveness (reduction in geometric mean gate count) for varying values of n and q, under a search timeout of 24 hours. The figure supports the tradeoff discussed above. Using too small values for n and q results in low effectiveness, and as we increase n or q effectiveness increases but then starts decreasing, as the negative impact of the large number of transformations starts outweighing their benefit. (See [33] for details about $|\mathcal{T}|$ for each configuration.) As expected, the optimal setting for n and q generally varies across circuits—smaller circuits tend to be better optimized with larger values of n [33]. Still, Figure 7 shows that there are several settings that yield good overall results: $3 \le n \le 6$ for $q = 3$, and $3 \le n \le 4$ for $q = 4$.[5]

Figure 8 shows how the search time impacts optimization for different choices for n (focusing on $q = 3$). For each value of n, we observe a quick initial burst, followed by a gentle increase. At the end of the initial burst, effectiveness monotonically decreases as n increases, for all $3 \le n \le 6$. As time progresses the gaps diminish and eventually the order is reversed: at around 21 hours $n = 6$ surpasses $n = 3$. The settings $n = 2$ and $n = 7$ yield poor effectiveness: $n = 2$ does not contain an adequate number of transformations and quickly saturates the search time, while $n = 7$ contains too many transformations and progresses too slowly.

Figure 8 also shows the effectiveness of a hypothetical run constructed by taking the best setting *for each circuit at each time*. This "best" curve considerably outperforms the others, because the best setting for n varies across circuits with different sizes.

[5]Interestingly, $q = 3$; $3 \le n \le 6$ cover the best optimization results for all circuits obtained among all configurations considered in Figure 7 [33].
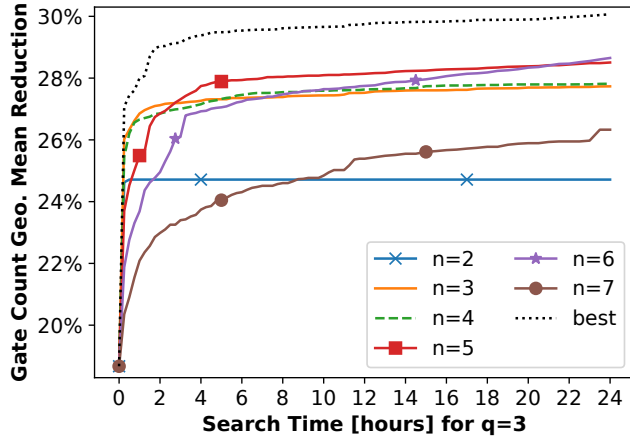
Figure 8. Optimization effectiveness over time (q=3; $2{\le}n{\le}7$). For each time point, "best" computes the reduction in geometric mean gate count obtained by selecting the most effective value for n at that time point for each circuit (i.e., different circuits may use different n's, and the same circuit may use different n's at different time points).

See [33] for more details, including plots akin to Figure 7 and Figure 8 for each circuit and a detailed results table.

8 Related Work

Quantum circuit compilation. Several optimizing compilers for quantum circuits have been recently introduced and are being actively developed: Qiskit [5] and t|ket⟩ [28] support generic gate sets; Quilc [29] is tailored to Rigetti Agave quantum processors; voqc [15] is formally verified in Coq. CertiQ [27] is a framework for writing and verifying Qiskit compiler passes. Nam et al. [23] develop heuristics tailored to the $\{H, X, R_z, CNOT\}$ gate set. Unlike Quartz, these systems rely on quantum-computing experts to design, implement, and verify transformations.

Quanto [25] automatically discovers transformations by computing concrete matrix representations of circuits. It supports parameters only by considering concrete values, and unlike Quartz, it does not discover or verify symbolic transformations, which are the source of many of the challenges Quartz deals with. Quanto uses floating-point matrix equality to identify equivalence between circuits, while Quartz uses a combination of fingerprinting, SMT-based verification, the RepGen algorithm, and other pruning techniques, which are needed since symbolic parameters greatly increase the number of possible circuits in the generation procedure.

Different from the aforementioned quantum optimizers that consider circuit transformations, PyZX [20] employs ZX-diagrams as an intermediate representation for quantum circuits and uses a small set of complete rewrite rules in ZX-calculus [13, 16] to simplify ZX-diagrams, which are finally converted back into quantum circuits.

While our approach builds on some of the techniques developed in prior work, Quartz is the first quantum circuit optimizer that can automatically generate and verify symbolic circuit transformations for arbitrary gate sets.

Superoptimization. Superoptimization is a compiler optimization technique originally designed to search for an optimal sequence of instructions for an input program [22]. Our approach to generating quantum circuit transformations by tracking equivalent classes of circuits is inspired by prior work in automatically generating peephole optimizations for the X86 instruction set [7, 14] and generating graph substitutions for tensor algebra [17, 30, 34].

TASO [17] is a tensor algebra superoptimizer that optimizes computation graphs of deep neural networks using automatically generated graph substitutions. TENSAT [34] reuses the graph substitutions discovered by TASO and employs equality saturation for tensor graph superoptimization. While Quartz draws inspiration from TASO and uses a similar search procedure, it is significantly different from prior superoptimization works because it targets quantum computing, which leads to a different semantics (i.e., using complex matrices) as well as a different notion of program equivalence (i.e., up to a global phase). Verifying quantum circuit transformations therefore uses different techniques compared to other superoptimization contexts. Applying equality saturation as in TENSAT [34] for optimizing quantum circuits is an interesting avenue for future work.

9 Conclusion and Future Work

We have presented Quartz, a quantum circuit superoptimizer that automatically generates and verifies circuit transformations for arbitrary gate sets with symbolic parameters. While Quartz shows that a superoptimization-based approach to optimizing quantum circuits is practical, we believe there are many opportunities for further improvement. As discussed in Section 7.5, Quartz's current search algorithm limits the number of transformations that can be effectively utilized. Improving the search algorithm may therefore lead to better optimization using (n, q)-complete ECC sets for larger values of n and q, which may also require improving the generator. Another limitation of Quartz that suggests an opportunity for future work is that it only targets the logical circuit optimization stage and does not consider qubit mapping. Applying superoptimization to jointly optimize circuit logic and qubit mapping is both challenging and promising.

Acknowledgments

References

[1] 2021. Qiskit ConsolidateBlocks. https://qiskit.org/documentation/stubs/qiskit.transpiler.passes.ConsolidateBlocks.html.

[2] 2021. Qiskit Optimize1qGates. https://qiskit.org/documentation/stubs/qiskit.transpiler.passes.Optimize1qGates.html.

[3] 2021. Rigetti Gates. https://pyquil-docs.rigetti.com/en/v2.7.0/apidocs/gates.html.

[4] 2022. The Quartz Quantum Circuit SuperOptimizer. https://github.com/quantum-compiler/quartz.

[5] Gadi Aleksandrowicz, Thomas Alexander, Panagiotis Barkoutsos, Luciano Bello, Yael Ben-Haim, David Bucher, Francisco Jose Cabrera-Hernández, Jorge Carballo-Franquis, Adrian Chen, Chun-Fu Chen, Jerry M. Chow, Antonio D. Córcoles-Gonzales, Abigail J. Cross, Andrew Cross, Juan Cruz-Benito, Chris Culver, Salvador De La Puente González, Enrique De La Torre, Delton Ding, Eugene Dumitrescu, Ivan Duran, Pieter Eendebak, Mark Everitt, Ismael Faro Sertage, Albert Frisch, Andreas Fuhrer, Jay Gambetta, Borja Godoy Gago, Juan Gomez-Mosquera, Donny Greenberg, Ikko Hamamura, Vojtech Havlicek, Joe Hellmers, Łukasz Herok, Hiroshi Horii, Shaohan Hu, Takashi Imamichi, Toshinari Itoko, Ali Javadi-Abhari, Naoki Kanazawa, Anton Karazeev, Kevin Krsulich, Peng Liu, Yang Luh, Yunho Maeng, Manoel Marques, Francisco Jose Martín-Fernández, Douglas T. McClure, David McKay, Srujan Meesala, Antonio Mezzacapo, Nikolaj Moll, Diego Moreda Rodríguez, Giacomo Nannicini, Paul Nation, Pauline Ollitrault, Lee James O'Riordan, Hanhee Paik, Jesús Pérez, Anna Phan, Marco Pistoia, Viktor Prutyanov, Max Reuter, Julia Rice, Abdón Rodríguez Davila, Raymond Harry Putra Rudy, Mingi Ryu, Ninad Sathaye, Chris Schnabel, Eddie Schoute, Kanav Setia, Yunong Shi, Adenilton Silva, Yukio Siraichi, Seyon Sivarajah, John A. Smolin, Mathias Soeken, Hitomi Takahashi, Ivano Tavernelli, Charles Taylor, Pete Taylour, Kenso Trabing, Matthew Treinish, Wes Turner, Desiree Vogt-Lee, Christophe Vuillot, Jonathan A. Wildstrom, Jessica Wilson, Erick Winston, Christopher Wood, Stephen Wood, Stefan Wörner, Ismail Yunus Akhalwaya, and Christa Zoufal. 2019. Qiskit: An Open-source Framework for Quantum Computing. https://doi.org/10.5281/zenodo.2562111

[6] Matthew Amy, Dmitri Maslov, and Michele Mosca. 2014. Polynomial-Time T-Depth Optimization of Clifford+T Circuits Via Matroid Partitioning. IEEE Transactions on Computer-Aided Design of Integrated Circuits and Systems 33, 10 (2014), 1476–1489. https://doi.org/10.1109/TCAD.2014.2341953

[7] Sorav Bansal and Alex Aiken. 2006. Automatic Generation of Peephole Superoptimizers. SIGOPS Oper. Syst. Rev. 40, 5 (Oct. 2006), 394–403. https://doi.org/10.1145/1168917.1168906

[8] Clark W. Barrett, Christopher L. Conway, Morgan Deters, Liana Hadarean, Dejan Jovanovic, Tim King, Andrew Reynolds, and Cesare Tinelli. 2011. CVC4. In Computer Aided Verification - 23rd International Conference, CAV 2011, Snowbird, UT, USA, July 14-20, 2011. Proceedings (Lecture Notes in Computer Science, Vol. 6806), Ganesh Gopalakrishnan and Shaz Qadeer (Eds.). Springer, 171–177. https://doi.org/10.1007/978-3-642-22110-1_14

[9] Alessandro Cimatti, Alberto Griggio, Ahmed Irfan, Marco Roveri, and Roberto Sebastiani. 2017. Satisfiability Modulo Transcendental Functions via Incremental Linearization. In Automated Deduction - CADE 26 - 26th International Conference on Automated Deduction, Gothenburg, Sweden, August 6-11, 2017, Proceedings (Lecture Notes in Computer Science, Vol. 10395), Leonardo de Moura (Ed.). Springer, 95–113. https://doi.org/10.1007/978-3-319-63046-5_7

[10] Leonardo de Moura and Nikolaj Bjørner. 2008. Z3: An Efficient SMT Solver. In Tools and Algorithms for the Construction and Analysis of Systems, 14th International Conference, TACAS 2008, Held as Part of the Joint European Conferences on Theory and Practice of Software, ETAPS 2008, Budapest, Hungary, March 29-April 6, 2008. Proceedings (Lecture Notes in Computer Science, Vol. 4963), C. R. Ramakrishnan and Jakob Rehof (Eds.). Springer, 337–340. https://doi.org/10.1007/978-3-540-

78800-3_24

[11] Yongshan Ding, Adam Holmes, Ali Javadi-Abhari, Diana Franklin, Margaret Martonosi, and Frederic T. Chong. 2018. Magic-State Functional Units: Mapping and Scheduling Multi-Level Distillation Circuits for Fault-Tolerant Quantum Architectures. In 51st Annual IEEE/ACM International Symposium on Microarchitecture, MICRO 2018, Fukuoka, Japan, October 20-24, 2018. IEEE Computer Society, 828–840. https://doi.org/10.1109/MICRO.2018.00072

[12] Eugene F Dumitrescu, Alex J McCaskey, Gaute Hagen, Gustav R Jansen, Titus D Morris, T Papenbrock, Raphael C Pooser, David Jarvis Dean, and Pavel Lougovski. 2018. Cloud quantum computing of an atomic nucleus. Physical review letters 120, 21 (2018), 210501.

[13] Amar Hadzihasanovic, Kang Feng Ng, and Quanlong Wang. 2018. Two Complete Axiomatisations of Pure-State Qubit Quantum Computing. In Proceedings of the 33rd Annual ACM/IEEE Symposium on Logic in Computer Science (Oxford, United Kingdom) (LICS '18). Association for Computing Machinery, New York, NY, USA, 502–511. https://doi.org/10.1145/3209108.3209128

[14] Stefan Heule, Eric Schkufza, Rahul Sharma, and Alex Aiken. 2016. Stratified Synthesis: Automatically Learning the X86-64 Instruction Set. In Proceedings of the 37th ACM SIGPLAN Conference on Programming Language Design and Implementation (Santa Barbara, CA, USA) (PLDI '16). Association for Computing Machinery, New York, NY, USA, 237–250. https://doi.org/10.1145/2908080.2908121

[15] Kesha Hietala, Robert Rand, Shih-Han Hung, Xiaodi Wu, and Michael Hicks. 2021. A Verified Optimizer for Quantum Circuits. Proc. ACM Program. Lang. 5, POPL, Article 37 (Jan. 2021), 29 pages. https://doi.org/10.1145/3434318

[16] Emmanuel Jeandel, Simon Perdrix, and Renaud Vilmart. 2018. A Complete Axiomatisation of the ZX-Calculus for Clifford+T Quantum Mechanics. In Proceedings of the 33rd Annual ACM/IEEE Symposium on Logic in Computer Science (Oxford, United Kingdom) (LICS '18). Association for Computing Machinery, New York, NY, USA, 559–568. https://doi.org/10.1145/3209108.3209131

[17] Zhihao Jia, Oded Padon, James Thomas, Todd Warszawski, Matei Zaharia, and Alex Aiken. 2019. TASO: Optimizing Deep Learning Computation with Automatic Generation of Graph Substitutions. In Proceedings of the 27th ACM Symposium on Operating Systems Principles (Huntsville, Ontario, Canada) (SOSP '19). Association for Computing Machinery, New York, NY, USA, 47–62. https://doi.org/10.1145/3341301.3359630

[18] Zhihao Jia, James Thomas, Todd Warzawski, Mingyu Gao, Matei Zaharia, and Alex Aiken. 2019. Optimizing DNN Computation with Relaxed Graph Substitutions. In Proceedings of the 2nd Conference on Systems and Machine Learning (SysML'19).

[19] Aleks Kissinger and John van de Wetering. 2019. Reducing T-count with the ZX-calculus. arXiv preprint arXiv:1903.10477 (2019).

[20] Aleks Kissinger and John van de Wetering. 2020. PyZX: Large Scale Automated Diagrammatic Reasoning. Electronic Proceedings in Theoretical Computer Science 318 (may 2020), 229–241. https://doi.org/10.4204/eptcs.318.14

[21] Jason R. Koenig, Oded Padon, and Alex Aiken. 2021. Adaptive restarts for stochastic synthesis. In PLDI '21: 42nd ACM SIGPLAN International Conference on Programming Language Design and Implementation, Virtual Event, Canada, June 20-25, 2021, Stephen N. Freund and Eran Yahav (Eds.). ACM, 696–709. https://doi.org/10.1145/3453483.3454071

[22] Henry Massalin. 1987. Superoptimizer: A Look at the Smallest Program. SIGARCH Comput. Archit. News 15, 5 (Oct. 1987), 122–126. https://doi.org/10.1145/36177.36194

[23] Yunseong Nam, Neil J Ross, Yuan Su, Andrew M Childs, and Dmitri Maslov. 2018. Automated optimization of large quantum circuits with continuous parameters. npj Quantum Information 4, 1 (2018), 1–12.

[24] M. Nielsen and I. Chuang. 2001. Quantum Computation and Quantum Information. Cambridge University Press.

[25] Jessica Pointing, Oded Padon, Zhihao Jia, Henry Ma, Auguste Hirth, Jens Palsberg, and Alex Aiken. 2021. Quanto: Optimizing Quantum Circuits with Automatic Generation of Circuit Identities. *arXiv:2111.11387* (2021). https://doi.org/10.48550/arXiv.2111.11387

[26] Matthew Reagor, Christopher B. Osborn, Nikolas Tezak, Alexa Staley, Guenevere Prawiroatmodjo, Michael Scheer, Nasser Alidoust, Eyob A. Sete, Nicolas Didier, Marcus P. da Silva, and et al. 2018. Demonstration of universal parametric entangling gates on a multi-qubit lattice. *Science Advances* 4, 2 (Feb 2018). https://doi.org/10.1126/sciadv.aao3603

[27] Yunong Shi, Runzhou Tao, Xupeng Li, Ali Javadi-Abhari, Andrew W. Cross, Frederic T. Chong, and Ronghui Gu. 2020. CertiQ: A Mostly-automated Verification of a Realistic Quantum Compiler. arXiv:1908.08963 [quant-ph]

[28] Seyon Sivarajah, Silas Dilkes, Alexander Cowtan, Will Simmons, Alec Edgington, and Ross Duncan. 2020. t|ket⟩: a retargetable compiler for NISQ devices. *Quantum Science and Technology* 6, 1 (Nov 2020), 014003. https://doi.org/10.1088/2058-9565/ab8e92

[29] Mark Skilbeck, Eric Peterson, appleby, Erik Davis, Peter Karalekas, Juan M. Bello-Rivas, Daniel Kochmanski, Zach Beane, Robert Smith, Andrew Shi, Cole Scott, Adam Paszke, Eric Hulburd, Matthew Young, Aaron S. Jackson, BHAVISHYA, M. Sohaib Alam, Wilfredo Velázquez-Rodríguez, c. b. osborn, fengdlm, and jmackeyrigetti. 2020. *rigetti/quilc: v1.21.0.* https://doi.org/10.5281/zenodo.3967926

[30] Haojie Wang, Jidong Zhai, Mingyu Gao, Zixuan Ma, Shizhi Tang, Liyan Zheng, Yuanzhi Li, Kaiyuan Rong, Yuanyong Chen, and Zhihao Jia.

2021. PET: Optimizing Tensor Programs with Partially Equivalent Transformations and Automated Corrections. In *15th USENIX Symposium on Operating Systems Design and Implementation (OSDI 21).* 37–54.

[31] Xin-Chuan Wu, Dripto M. Debroy, Yongshan Ding, Jonathan M. Baker, Yuri Alexeev, Kenneth R. Brown, and Frederic T. Chong. 2021. TILT: Achieving Higher Fidelity on a Trapped-Ion Linear-Tape Quantum Computing Architecture. In *IEEE International Symposium on High-Performance Computer Architecture, HPCA 2021, Seoul, South Korea, February 27 - March 3, 2021.* IEEE, 153–166. https://doi.org/10.1109/HPCA51647.2021.00023

[32] Mingkuan Xu, Zikun Li, Oded Padon, Sina Lin, Jessica Pointing, Auguste Hirth, Henry Ma, Jens Palsberg, Alex Aiken, Umut A. Acar, and Zhihao Jia. 2022. *Artifact for PLDI 2022 paper: Quartz: Superoptimization of quantum circuits.* https://doi.org/10.5281/zenodo.6508992

[33] Mingkuan Xu, Zikun Li, Oded Padon, Sina Lin, Jessica Pointing, Auguste Hirth, Henry Ma, Jens Palsberg, Alex Aiken, Umut A. Acar, and Zhihao Jia. 2022. Quartz: Superoptimization of quantum circuits (extended version). arXiv:2204.09033 [cs.PL]

[34] Yichen Yang, Phitchaya Phothilimthana, Yisu Wang, Max Willsey, Sudip Roy, and Jacques Pienaar. 2021. Equality Saturation for Tensor Graph Superoptimization. In *Proceedings of Machine Learning and Systems*, A. Smola, A. Dimakis, and I. Stoica (Eds.), Vol. 3. 255–268.